JOURNAL OF SPACECRAFT AND ROCKETS
Vol. 45, No. 4, July–August 2008

Evaluation of Kinetic/Continuum Solver for Hypersonic Nozzle-Plume Flow

Eswar Josyula*
U.S. Air Force Research Laboratory, Wright–Patterson Air Force Base, Ohio 45433
Robert R. Arslanbekov† and Vladimir I. Kolobov‡
CFD Research Corporation, Huntsville, Alabama 35805
and
Sergey F. Gimelshein§
University of Southern California, Los Angeles, California 90089

DOI: 10.2514/1.35431

The objective of this study is to evaluate the predictive capability and numerical efficiency of a newly developed combined kinetic/continuum approach incorporated in the unified flow solver in application to complex expanding nozzle-plume flows. The results of numerical simulations of a steady-state nitrogen flow expanding from a hypersonic nozzle into a low-density stagnant gas are presented. The Euler equations are solved in high-density continuum regions, whereas the direct solution of the Boltzmann equation is conducted in the low-density noncontinuum regions. The appropriate set of equations, kinetic or continuum, are solved using a dynamically adaptive mesh and an automatic domain decomposition feature. The nozzle rotational and vibrational temperature predictions are compared with existing temperature data obtained in the NASA Electric Arc Shock Tube facility. A direct simulation Monte Carlo solver, SMILE, was run for the plume domain to provide a reference numerical solution. Detailed comparison of united flow solver predictions of plume macroparameters with those of SMILE is satisfactory in the majority of the flowfield; in other parts, however, the differences are significant and clearly demonstrate the need for proper treatment of the numerical parameters in the two methodologies.

Introduction

BEFORE the 1960s, ballistic Earth entries were not a major challenge to the computational fluid dynamics (CFD) community because the requirements were such that the vehicles quickly passed the most complicated transitional flow regime in the 80–100 km altitude range. However, with the recent Space Transportation System (STS) missions, the transatmospheric flight with hypersonic winged vehicles, as well as considering the space missions proposed by various nations, the subject of rarefied-transitional-continuum flow has experienced a renewed interest [1–4]. Another important example of the continuum-rarefied flow regimes is the high-altitude plume. The assessment of interaction between the spacecraft and the plume requires an accurate description of the resulting flowfield [5]. The numerical modeling of such flows is complicated because of the changing flow regimes, from continuum near the nozzle throat to free molecular at large distances from the nozzle, with the transitional regime between them [6]. From earlier studies, it is noted that the difficulty of modeling thermochemical nonequilibrium in mixed continuum and rarefied regimes of the gas is exacerbated by the difficulty in treating the interfaces between the continuum and rarefied regions in the domain of interest.

Presented as Paper 209 at the 45th AIAA Aerospace Sciences Meeting and Exhibit, Reno, NV, 8–11 January 2007; received 6 November 2007; revision received 24 January 2008; accepted for publication 4 February 2008.

*Senior Research Aerospace Engineer, 2210 Eighth Street. Associate Fellow AIAA.
†Principal Scientist, Plasma Technologies Group, 215 Wynn Drive.
‡Manager, Plasma Technologies Group, 215 Wynn Drive. Member AIAA.
§Research Assistant Professor, Department of Aerospace and Mechanical Engineering, 201 Rapp Research Building. Member AIAA.

The Knudsen number, based on local gradients of flow properties, is a measure of the local departure from equilibrium. Even though the rarefied gas flow is typically associated with large Knudsen numbers, the nonequilibrium conditions related to large property gradients also occur in certain regions of continuum flow [7], such as inside shock waves and mixing layers, Knudsen layers near the boundaries, and sharp leading edges of hypersonic vehicles. Other important examples of highly nonequilibrium phenomena in gas and vapor systems include [8,9] plasma-enhanced chemical vapor deposition and etching at low gas pressures, the microelectromechanical systems due to their small sizes, the interactions of space vehicles with space environments in the presence of electric and magnetic fields, and finally, spacecraft thrusters and Earth entry vehicles.

The particle method known as direct simulation Monte Carlo (DSMC) is widely used today for modeling the high Knudsen number rarefied flows in which the continuum description based on Euler/Navier–Stokes equations breaks down [10,11]. The DSMC method tracks a large number of statistically representative particles, whose motion and interactions are used to modify their position, velocities and, where applicable, the reactive properties during chemical reactions in the flowfield. DSMC decouples the molecular motions from the intermolecular collisions over small time intervals. For a large enough number of simulated particles (as the number tends to infinity), the DSMC method has been shown to be equivalent to the solution of the Boltzmann kinetic equation for a monatomic gas with binary collisions [12,13]. In the DSMC method, the computational time step must be less than the mean collision time, and computational cells should be smaller than the mean free path of the gas particles. It is well known that DSMC becomes impractical for high density when the large number of computational cells and small time steps are required (see, for example, [14]).

The development of hybrid methods coupling atomistic scale models such as the DSMC with continuum models has been an important area of research over the last decade [3,15]. The statistical noise of particle methods is a serious shortcoming of hybrid solvers based on DSMC, both low-speed flows [16] and, to a lesser extent, supersonic flows [17]. The statistical noise is problematic in hybrid solvers based on DSMC and has been a subject of research in the past

(see, for example, [18]). These deficiencies in particle methods are overcome using direct numerical solution of the Boltzmann equation, which has been shown to be a viable alternative to DSMC for both subsonic flow simulations [19] and high-density hypersonic flow simulations [20].

The principal advantage of equation-based (integro-differential Boltzmann equation and the partial differential equations of Navier–Stokes and Euler) hybrid solvers for computing mixed continuum-rarefied flows is that the coupling between the continuum and kinetic noncontinuum solvers can be handled at the interfaces with much greater ease. This is particularly true when the continuum Navier–Stokes and Euler equations are solved using gas-kinetic schemes using the distribution function. The single computational tool using automatic domain decomposition into noncontinuum and continuum parts is intended to compute flowfields having mixed regions of continuum, transitional, and rarefied regimes [21–24].

The last decade has seen a resurgence of direct methods for the numerical solution of the Boltzmann equation, describing the evolution of the particle velocity distribution function in phase space [25–28]. The Boltzmann equation methods spurred the development of kinetic schemes for solving continuum equations of gas dynamics. Among such schemes are gas-kinetic schemes with multitemperature continuum models derived from the Boltzmann equation using a first-order Chapman–Enskog expansion of an anisotropic velocity distribution function. The model, extended to rotational nonequilibrium, was applied to highly nonequilibrium shock wave structures and compared favorably with DSMC solutions and experimental data. The equations with generalization of the dissipative coefficients based on the closed form solution of the Bhatnagar–Gross–Krook (BGK) model of the Boltzmann equation were employed in some of these gas-kinetic numerical schemes. Calculations of the normal shock wave structure for monatomic and diatomic gases in the Mach number range from 1.2 to 12.9 was found to give satisfactory results [29,30].

These new techniques have been combined in a unified kinetic/continuum flow solver (UFS) developed using adaptive mesh and algorithm refinement (AMAR) methodology [24]. The UFS uses direct the numerical solution of the Boltzmann equation in the kinetic parts of the flow and gas-kinetic CFD schemes in the continuum parts of the flow. UFS automatically detects the continuum and kinetic regimes using continuum breakdown criteria and invokes the appropriate solvers for different parts of the flowfields. The dynamic grid adaption and automatic introduction and removal of kinetic patches provide significant savings by limiting molecular scale solutions only to the regions where they are needed. The UFS has been validated and demonstrated for a variety of single-component flows over a wide range of Knudsen and Mach numbers and extended to multicomponent flows of atomic gases [31]. Extensions to molecular gases with internal degrees of freedom have been reported in [20,32].

An important flow problem that is difficult to simulate numerically is the nozzle-plume flow at high altitudes involving the interaction of high-density nozzle plume with the surrounding rarefied atmosphere. Such an interaction is characterized by a number of important physical phenomena. Rarefied plume expansion results in cooling of molecules downstream of the nozzle exit. The molecular cooling along the streamlines results in differences of translational temperatures in the axial and radial directions, with the axial temperatures higher along the nozzle axis and the radial temperatures higher at increasing angles from the axis. Additional peculiarities appear in molecular gases. Because of the finite rates of rotational and vibrational relaxation, the rapid reduction of translational temperature results in rotational and vibrational temperatures lagging the translational temperature downstream of the plume. Because of slow vibrational relaxation, vibrational modes become essentially frozen during gas expansion into the low-density region.

The interaction of the plume molecules with the freestream molecules results in the formation of a hot mixing layer, whose location depends primarily on the degree of plume underexpansion. The increase in the translational temperature and the temperatures in the internal energy modes in the mixing layer depends on the degree of rarefaction of the surrounding atmosphere. Inside the mixing layer in the nearly free molecular regime, the nonequilibrium is restricted to the translational energy, the temperature increase caused by the interpenetration of two molecular fluxes. For near-continuum flow, however, the friction between the freestream and the plume increases the translational temperatures, and subsequent translation-rotation energy transfers increase rotational temperature, which typically lags the translational temperature. The vibrational relaxation, frozen in the axial direction in the plume, may somewhat accelerate in the mixing layer, affecting the otherwise gradual increase of vibrational temperature from its freestream value to the temperature in the mixing layer. All these flow phenomena make underexpanded plume flow an appropriate, although somewhat complex, problem for verification and validation of numerical approaches and physical models, which is the main scope of the present study.

The present study aims to further evaluate the accuracy and performance of the coupled continuum/kinetic approach of the UFS for nozzle-plume flows through detailed comparisons with experimental data inside the nozzle and DSMC solutions in the mixed continuum-rarefied plume region. A high-density nozzle test case was selected for this study due to availability of experimental data of rotational and vibrational temperatures measurements along the nozzle axis in the NASA Electric Arc Shock Tube (EAST) facility [33]. A DSMC code (SMILE) was used in the plume region to provide reference solution of the complex flow of the high-density nozzle flow exiting into a low-density stagnant gas resulting in a plume interacting with the background gas.

Numerical Approach

This section describes the numerical approach used in UFS and SMILE. Here we outline the overall structure of the UFS and describe only the recently developed capabilities important for the particular problem studied in this paper. The UFS uses direct numerical solution of the Boltzmann transport equation (DNS-B) to describe gas dynamics at atomistic scale. The Boltzmann equation has the form [27]

$$\frac{\partial f}{\partial t} + \nabla_{\mathbf{r}} \cdot (\boldsymbol{\xi} f) = I(f, f) \tag{1}$$

where $\mathbf{r}$ is the position vector in physical space, $\boldsymbol{\xi}$ is the velocity vector, and t is the time. The distribution function $f(t, \mathbf{r}, \boldsymbol{\xi})$ is the molecular number density in a six-dimensional phase space formed by the three velocity and three space coordinates. The right-hand side of Eq. (1) contains an integral operator describing the effect of binary collisions on the distribution function.

For the numerical solution of Eq. (1), a Cartesian mesh in velocity space is introduced with a cell size of $\delta\xi$ and nodes $\boldsymbol{\xi}_i$. Using this mesh, Eq. (1) is reduced to a set of linear hyperbolic transport equations in physical space with a nonlinear source term:

$$\frac{\partial f_i}{\partial t} + \nabla_{\mathbf{r}} \cdot (\boldsymbol{\xi} f_i) = I(f_i, f_i) \tag{2}$$

The collision operator I written in terms of impact parameters is

$$I(\boldsymbol{\xi}) = \int_0^{2\pi} \mathrm{d}\epsilon \int_0^{b_m} \mathrm{d}b \int [f(\boldsymbol{\xi}_1') f(\boldsymbol{\xi}') - f(\boldsymbol{\xi}_1) f(\boldsymbol{\xi})] g b \, \mathrm{d}\boldsymbol{\xi}_1 = -\nu f + G \tag{3}$$

where b is the impact parameter usually bounded by a certain value b_m, ϵ is the azimuth impact angle, and $g = |\boldsymbol{\xi}_1 - \boldsymbol{\xi}|$. The postcollision velocities $(\boldsymbol{\xi}', \boldsymbol{\xi}_1')$ and the precollision velocities $(\boldsymbol{\xi}', \boldsymbol{\xi}_1')$ satisfy the momentum and energy conservation laws. The particular form of the collision frequency (ν) and inverse collision term (G) depend on the intermolecular interaction potential. We use conservative methods [24] to calculate contributions of individual collisions. The multidimensional integrals were evaluated using Korobov sequences [34]. The hard-sphere, Lennard Jones, and Coulomb collision models have been implemented. The simple BGK model has been used as well due to its efficiency. Table 1 summarizes

Table 1 UFS solver attributes. 1) Adaptive mesh and algorithm refinement (AMAR) capabilities, dynamic load balancing for multiprocessor simulations common to all solvers, 2) several options of intermolecular interactions for the Boltzmann collision integral hard-sphere, Lennard Jones, Maxwell, inverse power, and Coulomb potentials, 3) BGK collision integral with Prandtl number correction, and 4) the kinetic solver considers the Boltzmann equation in phase space as 3-D in physical space with three velocity components

	Kinetic solver		Continuum solver	
	Boltzmann collision integral	BGK collision integral	Navier–Stokes gas-kinetic scheme	Euler gas-kinetic scheme
3-D/2-D planar	Yes	Yes	Yes	Yes
2-D axisymmetric	No	Yes[a]	No	Yes[a]
Rot. nonequil., 2T	No	Yes[a]	No	Yes[a]
Vib. nonequil. 3T	No	Yes[a]	No	Yes[a]
Nonreacting gas mixtures	Yes	Yes	No	Yes
Reacting mixtures	No	No	No	Yes

[a]Represents specific capabilities used in the current study.

the different capabilities in UFS solver and the specific solvers invoked for the present paper.

The numerical solution of Eq. (2) is split into two stages: free motion and collisions [7]. The integration of the partial differential equation can be performed using numerical methods of the continuum gas dynamics. The advantage of equation-based kinetic approach compared with particle-based methods (such as DSMC) is the possibility of using explicit or implicit CFD numerical algorithms and different types of computational mesh in physical space. The explicit finite volume formulation of the collisionless part of Eq. (2) can be written as

$$V\frac{\left(f_{ij}^{*k}-f_{ij}^{k-1}\right)}{\Delta t}+\sum_{\text{face}}(\boldsymbol{\xi}_i\cdot\mathbf{n})_{\text{face}}f_{i,\text{face}}^{k-1}S_{\text{face}}=0 \tag{4}$$

where j denotes cell number in physical space. Here k is the time index, $*$ denotes the intermediate level, $f_{i,\text{face}}^{k-1}$ is the value of the function on the cell face, $\mathbf{n}$ is the outward normal vector to the face, V is the cell volume, and S_{face} is the face surface area. For calculation of the face values of the distribution function, standard interpolation schemes of first and second order have been used in UFS. The second-order scheme has three options: 1) no limiter, 2) the minmod limiter, and 3) van Leer limiter. UFS uses a binary tree-based dynamically adaptive isotropic Cartesian grid with a local mesh size h. The grid is automatically generated in a computational domain with embedded boundaries using the GFS engine [35].

The relaxation stage also uses explicit scheme with automatic selection of the time step:

$$\frac{f_{ij}^{k}-f_{ij}^{k-1}}{\Delta t}=-\nu_{ij}^{*k}f_{ij}^{*k}+G_{ij}^{*k} \tag{5}$$

For the present study, the transport and collisional relaxation are computed as two stages. However, it is worth noting that with conservatively calculated collision integrals, it is possible to use the computational scheme without the transport/relaxation splitting. This could be particularly useful for highly collisional flows. Further details on the models used in the kinetic/continuum approach of UFS can be found in [24].

The continuum flow solver used in the present study is based on the kinetic-Euler scheme, which follows the equilibrium flux method (EFM) by Pullin [36]. The internal energy modeling of rotational and vibrational relaxation is implemented in the kinetic-Euler scheme. The various solvers in UFS and their attributes are summarized in Table 1. The attributes marked with asterisk in Table 1 are used in the present nozzle-plume study. For the present study, the continuum solver in UFS means the kinetic-Euler solver. Reference to the Boltzmann solver in UFS is made for simulations of flowfield in noncontinuum regions. UFS solver referenced in the paper means that both continuum and Boltzmann solvers are used as required by the flowfield.

Internal Energy Excitation in UFS

The internal energy associated with the rotationally and vibrationally excited molecules can be implemented in primarily two ways. The state-to-state kinetic approach, demonstrated for the shock wave problem in [20], is for rotational nonequilibrium. The state-to-state approach solves a kinetic equation for each excited level and is computationally expensive. The other, a more simplified approach of modeling the internal energy, was taken in the present study. In the present study, we extended the Rykov model (R model) [37], which was demonstrated to be efficient and accurate in a number of studies on rotational excitation (see [38] and references therein). The R model reduces the kinetic equation to a set of two kinetic equations in the form

$$\frac{\partial f_0}{\partial t}+\nabla\cdot(\boldsymbol{\xi}f_0)=\nu_r\left(f_0^r-f_0\right)+\nu_t\left(f_0^t-f_0\right) \tag{6}$$

$$\frac{\partial f_1}{\partial t}+\nabla\cdot(\boldsymbol{\xi}f_1)=\nu_r\left(f_1^r-f_1\right)+\nu_t\left(f_1^t-f_1\right) \tag{7}$$

where the relaxation frequencies ν_r and ν_t are determined from gas viscosity through a parameter Z_R describing the number of elastic collisions that occur for each rotational collision. The distribution functions f_0^r, f_0^t, f_1^r, and f_1^t are related through the ratio of elastic-to-nonelastic collisions Z_r [38–40]. The vibrational-translational exchange rates in UFS were taken from the work of Millikan and White [41]. Further details of this approach can be found in [32].

Coupling Continuum and Kinetic Domains in UFS

The UFS is a fully coupled method of continuum and noncontinuum solvers in which the boundary conditions are automatically updated as the solution advances in time and reaches a steady state. The continuum and kinetic domains are automatically detected in the UFS solver and the appropriate solver used. The initial conditions dictate the choice of the solver (kinetic-Euler or Navier–Stokes, BGK or full Boltzmann) at the outset of the calculations. The switching of the solver takes place based on the criterion determined from the following equation:

$$S_\rho=Kn\frac{1}{\rho}|\nabla\rho| \tag{8}$$

where ρ is the mass density and Kn is the local Knudsen number. If S is greater than some threshold value, the kinetic Boltzmann solver is used. Numerical experiments show that the heat flux is more sensitive than pressure for different values of the S parameter. For an extended rarefied region, the S values converge for various small values. Decreasing S value, however, would incur greater computational cost. The typical range for S can be from 0.1 to 0.001. The values of S used in the present study are 0.025, 0.033, and 0.04.

The coupling of the Boltzmann and Euler solvers is as follows. The boundary conditions for the Euler equations are determined from the moments of the velocity distribution function in the two

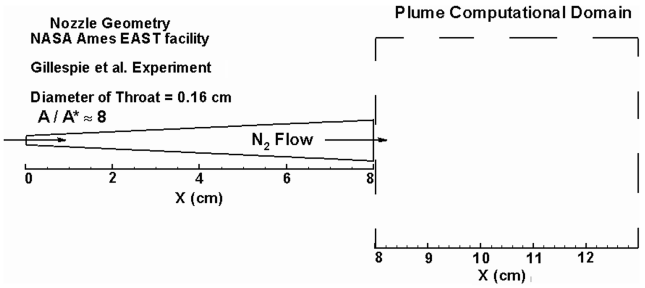

Fig. 1 Nozzle geometry adapted for experiments in NASA's EAST facility and plume computational domain at nozzle exit.

neighboring cells. From the known velocity distribution function, parameters of the corresponding Maxwellian distribution are defined. The boundary conditions for the Boltzmann equation are obtained assuming Maxwellian velocity distribution function in the continuum cells. Table 1 shows the details of the various solvers and the specific features marked by asterisk in the Table used in the present study.

Details of SMILE (DSMC) Solver

The benchmark numerical solutions were obtained with a direct simulation Monte Carlo method solver SMILE [42]. The axisymmetric capability of the DSMC-based code SMILE has been used in this work. The relevant features of SMILE are parallel capability, different collision and macroparameter grids with automatic adaptations, and spatial weighting. Spatial weighting is radial, with different weights assigned to different horizontal rows of background cells. The total number of rows is 100, and a weight of 1 was assigned to the innermost 10 layers to avoid any nonphysical, numerical effects associated with spatial weights near the nozzle axis. The total number of collision cells were varied from 1 to 3 million, and simulated particles were varied from 4 to 12 million. There was no noticeable effect of the variation in number of cells and molecules on the flowfield. The results presented in this study are for 12 million molecules and 3 million cells.

The majorant frequency scheme [43] was used to calculate intermolecular interactions. The intermolecular potential was assumed to be a variable hard sphere [10]. Energy redistribution between the internal (rotational and vibrational) and translational modes was performed in accordance with the Larsen–Borgnakke model [44]. Temperature-dependent relaxation numbers were used in the present study. For rotational relaxation, an expression given in [45] was used with the DSMC correction described in [46]. For vibrational relaxation, a semiempirical expression [41] with a high-temperature term [47] was used with the DSMC correction [48]. A particle-selection methodology prohibiting double relaxation [49] was used to provide meaningful rotational and vibrational relaxation rates. For the background pressure case, a background pressure of 10^{23} molecule/m^3 was chosen. The DSMC computations ran with a time step size of 0.25 ns. The macroparameter sampling was started after 200,000 time steps in the SMILE code.

Flow Conditions of Numerical Simulation

The nozzle experiments conducted in the NASA Ames EAST facility were numerically simulated by Gillespie et al. [50] on a computational grid that was a quasi-one-dimensional adaptation of the two-dimensional nozzle. The area ratios of the quasi one-dimensional adaptation of [50] were used in the present study to generate the nozzle grid for the numerical studies. The nozzle profile is shown in Fig. 1, and the nozzle area ratio is 8. The test gas is nitrogen; the mass fraction of nitrogen atoms at the throat was set to 1.0E − 4. The flow conditions at the nozzle throat are as follows: $T_0 = 2800$ K, $p_0 = 10,335.1$ kPa. The computational domain of the high-density nozzle was extended beyond the exit plane to simulate the plume flow. The UFS was used with the following subsystems: 1) a kinetic-continuum-Euler approach, 2) a hybrid approach that chooses the kinetic continuum or the Boltzmann solver based on the breakdown criterion. The SMILE code was employed in the plume region only, with the inflow conditions of the plume extracted from the given UFS solution at the nozzle exit.

Initial and Boundary Conditions

Nozzle boundary conditions for the continuum solver are as follows. The flow is assumed to be in equilibrium at the throat of the nozzle and given by the experimental reservoir conditions. At the symmetry axis, a symmetry condition was used. At the exit boundary, the flow variables were extrapolated. The inflow conditions for the plume simulations in UFS and SMILE (DSMC) were taken from the continuum simulations of the flow inside the nozzle, for the geometry presented in Fig. 1. These conditions are the number density 1×10^{25} m^{-3}, the axial velocity 1900 m/s, the translational and rotational temperatures set as 800 K, and vibrational temperature is 2400 K. It was assumed that the plume region is initially occupied by some background gas with a density of 1/100th of the nozzle exit density, zero velocity, and a temperature of 300 K. At the left boundary of the computational domain, background gas parameters were set to maintain the initial background gas, and the bottom boundary was assumed to be one of symmetry. At the other boundaries, free exit (extrapolation) boundary conditions have been set. A specular reflection boundary condition at the wall of the nozzle was specified for the UFS solver. In SMILE computations, the plume inflow boundary conditions are specified at a starting surface located along the nozzle exit. At this surface, a Maxwellian distribution function was used for molecular velocities, and a Boltzmann distribution was assumed for internal, rotational, and vibrational energies of molecules. The radially varying parameters of these distributions were obtained from the UFS continuum computations. At the outflow boundaries, a Maxwellian distribution with the background gas parameters was assumed.

Computer Resource Requirements

A summary of grid/cell details and the computational resources used by UFS and SMILE is given in Tables 2 and 3. Three UFS computations and one SMILE computation were conducted and are listed in the tables. The velocity grid shown for the UFS runs is needed for kinetic cells only and not for continuum cells. The Cartesian velocity points in the UFS were the same at all spatial coordinates and do not vary from cell to cell. It was made sure that the UFS solution did not change when the velocity grid points were doubled, which is explained by the fact that the simulated distribution function was adequately represented by the velocity grid used. A similar study was conducted by increasing the UFS physical grid size to ensure grid convergence.

Table 2 Grid size/cells details for UFS and SMILE (DSMC) for high-density plume with the stagnation properties: $T_0 = 2800$ K, $p_0 = 10,335.1$ kPa, [33]

Type solver	Type config	Physical grid size	Velocity grid size	No. of molecules	Kinetic cells (no.)	Continuum cells (no.)
UFS (computation 1)	2-D/Axi	13,400	32 × 32 × 16	n/a	3600	9800
UFS (computation 2)	2-D/Axi	14,200	32 × 32 × 16	n/a	5520	8680
UFS (computation 3)	2-D/Axi	225,560	20 × 20 × 10	n/a	35,603	190,000
SMILE (computation 4) (DSMC)	2-D/Axi	3 million cells	n/a	12 million molecules	n/a	n/a

Table 3 Computer resources used by UFS and SMILE for high-density plume with nozzle conditions $T_0 = 2800$ K, $p_0 = 10,335.1$ kPa, [33]

Type solver	Processor speed	No. of processors	Memory MB (max)	Total simulation time
UFS (computation 1)	2.8 GHz	24	1131	72 h
UFS (computation 2)	2.8 GHz	24	1260	120 h
UFS (computation 3)	2.8 GHz	128	1296	512 h
SMILE (computation 4) (DSMC)	2.8 GHz	14	500	420 h

Note that the total simulation (computational) time is the product of wall clock time and the number of processors. The computer resource requirements of the UFS (computation 3) is 1.2 times higher simulation (computational) time and 2.6 times the memory than that used by SMILE. Because UFS has the option of starting and stopping the Boltzmann solution at any time during a simulation, it is possible to run the continuum solver in the entire domain until it is converged, and then obtain the Boltzmann solution only in the kinetic domain, which is coupled to the rest of the continuum domain. For the computations 1 and 2 listed, the continuum solver was run for the first 7000 time steps, which took about a minute on the 24 processor cluster, and then the Boltzmann solver was started in the kinetic domain. For the UFS computation 3, the solution ran for 21,000 time steps for the continuum solver (which was about 10% of the total computational time) and 2000–3000 time steps for the Boltzmann solver to converge. The UFS is a fully coupled method, and the boundary conditions at the kinetic-continuum interfaces are automatically updated as the solution advances in time and reaches a steady state. The comparisons of results using UFS computation 3 with the reference SMILE solution are shown in the Results Section.

Results and Discussion

UFS Simulations in Nozzle and Plume

The results of UFS simulations using the gas-kinetic-continuum solver are shown in Fig. 2. Figure 2 shows UFS-predicted translational (T_t) and vibrational temperatures (T_v) and experimental rotational (T_r) and vibrational temperature measurements in the nozzle section. The UFS prediction of translational temperature is very close to the experimental rotational temperature measurements at the two nozzle locations of approximately 4 and 6 cm. The vibrational temperature prediction is essentially frozen along the nozzle centerline and within the uncertainty of the experimental measurements. In this connection, note that the vibrational-translational exchange rates implemented in UFS were taken from the work of Millikan and White [41], and as reported in an earlier work [51], slower vibrational–translational (V–T) rates of Blackman [52] cause the vibrational temperatures predictions to be lower by about 7%. The dashed line represents the translational and vibrational temperatures along the nozzle axis (the solid line shows the extension beyond the nozzle exit plane of 8 cm) that will be discussed in the next section.

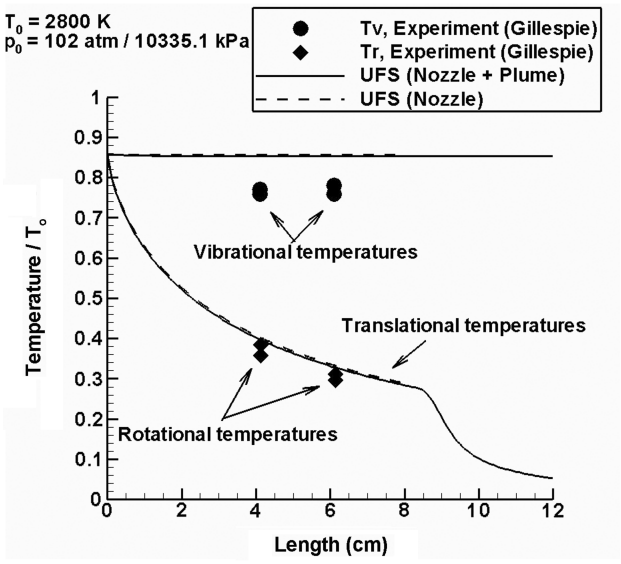

Fig. 2 Comparison with experiment: temperatures along centerline length of nozzle and plume. $T_0 = 2800$ K, $p_0 = 10,335.1$ kPa.

Figures 3–6 obtained by UFS show contours of density, translational temperature, and Mach number inside the nozzle and plume. The density, Fig. 3, in the nozzle throat is about an order of magnitude higher than in the plume region. The translational temperature, Fig. 4, is highest at the nozzle throat. As the flow expands through the nozzle, the temperature sees a sharp decrease in the nozzle. There is, however, an increase in translational temperature in the region of the plume mixing layer, formed by the nozzle exit gas turning upwards, away from the centerline, and interacting with the background gas. Vibrational temperature, Fig. 5, is essentially frozen in the nozzle and near the centerline of the plume downstream. However, the region above the mixing layer in the plume where the flow slows down exhibits a decrease in vibrational temperature by an order of magnitude caused by vibrational-translational exchanges. The flow Mach number (Fig. 6) increases as the flow expands in the nozzle and in the plume. The region above the mixing layer, however, shows a marked reduction in the flow Mach number due to the interaction between the plume and the stagnant background gas.

Two important features of UFS solver, the adaptive gridding of the Cartesian mesh in the plume flowfield and the feature on automatic detection of continuum-kinetic regimes of UFS, are shown in Figs. 7 and 8. The grid adaptation shown is based on local gradients of density and velocities (u and v components). The Cartesian grid used in UFS, Fig. 7, shows increased grid adaptation for higher flow gradients, particularly so in the mixing layer. The upstream region away from the centerline leading to the mixing layer has greater grid densities than downstream. Figure 8 shows the UFS feature of automatic detection of kinetic and continuum regions in the flowfield. The kinetic region depicted in black was solved in UFS by the Boltzmann solver, and the continuum region shown in white by the gas-kinetic-continuum solver, the kinetic and continuum regions depicting the relative measure of rarefaction. The computational cost required by UFS in the kinetic vs continuum regions is estimated as follows: a third of the simulated domain requires kinetic calculations with the rest of the domain treated as continuum. Figure 9 shows the Knudsen number in the plume, an indication of the region in which the continuum equations will fail and a kinetic solver would be necessary.

UFS and SMILE Comparisons in the Plume Domain

This section shows detailed comparison of flow predictions obtained by UFS (continuum and kinetic solvers) and SMILE (DSMC) for comparisons of density, translational, vibrational and rotational temperatures, and Mach number in Figs. 10–19. Figures 10 and 11 show the comparison of number density contours in the plume region for UFS and SMILE. Both solvers predict a very similar flowfield, both qualitatively and quantitatively.

The translational temperature contours predicted by UFS and SMILE in the plume region are shown in Figs. 12 and 13, respectively. The mixing layer predicted by the Boltzmann solver of UFS has slightly higher temperatures near the nozzle exit. Both codes predict the mixing layer at an angle of about 40 deg. The general trends of the temperature flowfields by both solvers are very similar. The SMILE contours are smeared near the nozzle, evidence of the

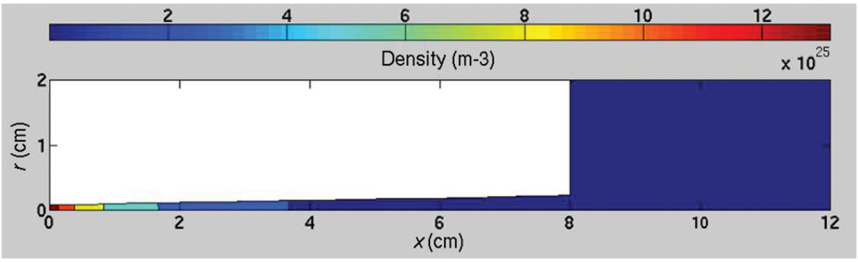

Fig. 3 Nozzle and plume density contours using UFS.

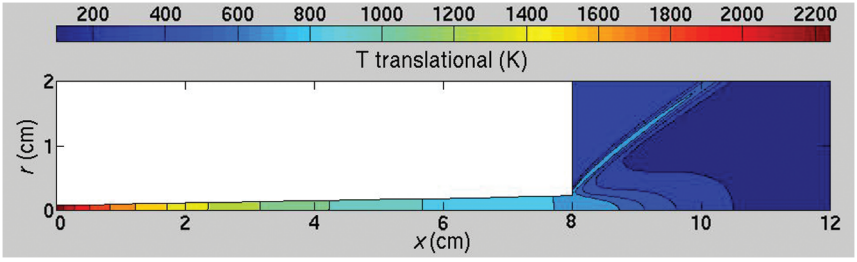

Fig. 4 Nozzle and plume translational temperature contours using UFS.

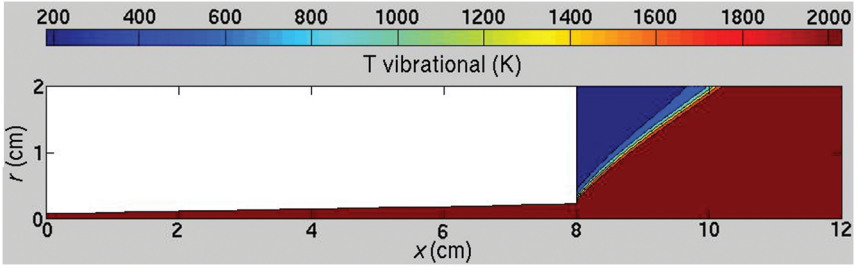

Fig. 5 Nozzle and plume vibrational temperature contours using UFS.

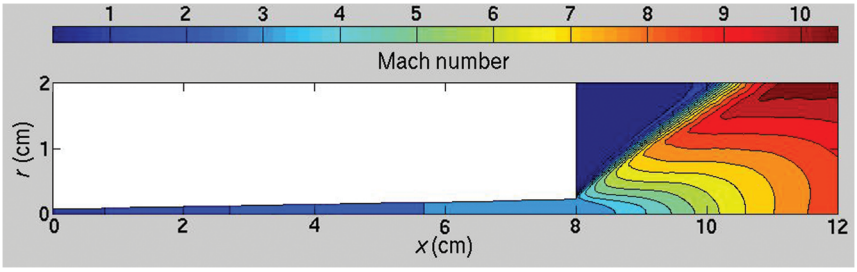

Fig. 6 Nozzle and plume Mach number contours using UFS.

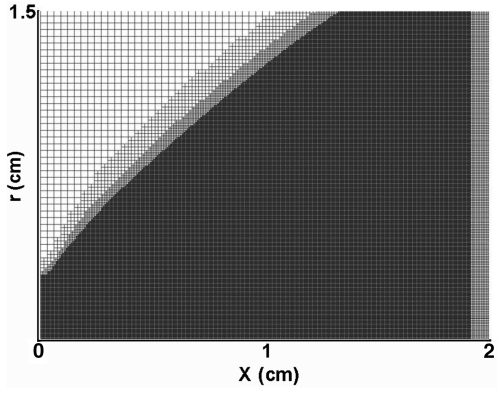

Fig. 7 Plume grid in UFS showing Cartesian grid cells with adaptive gridding.

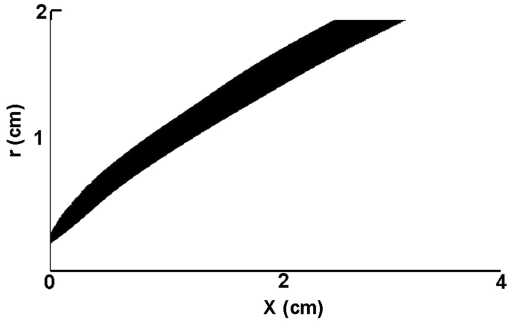

Fig. 8 Plume grid and kinetic/continuum flag in UFS using automatic detection showing kinetic and continuum domain. The black domain represents the kinetic, whereas the rest of the domain is continuum.

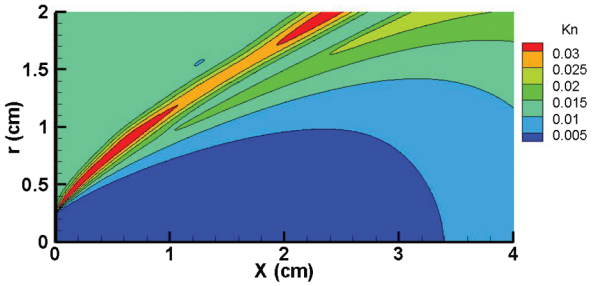

Fig. 9 Knudsen number contours using UFS.

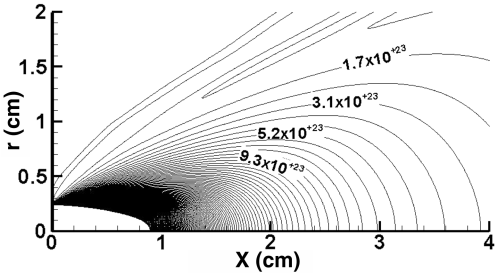

Fig. 10 Plume density contours using UFS.

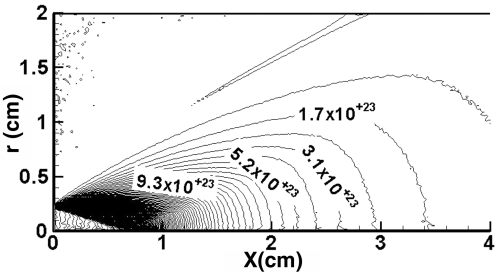

Fig. 11 Plume density contours using SMILE (DSMC).

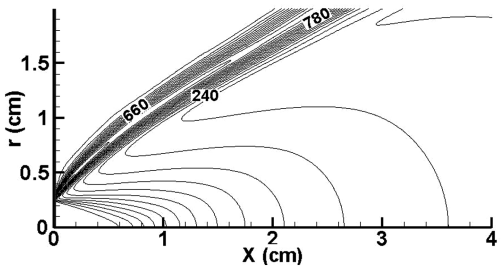

Fig. 12 Plume translational temperature contours using UFS.

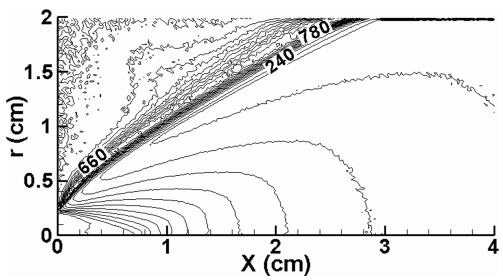

Fig. 13 Plume translational temperature contours using SMILE (DSMC).

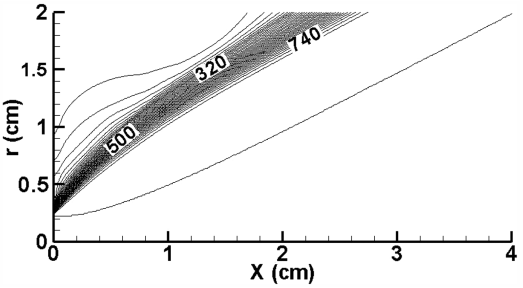

Fig. 14 Plume vibrational temperature contours using UFS.

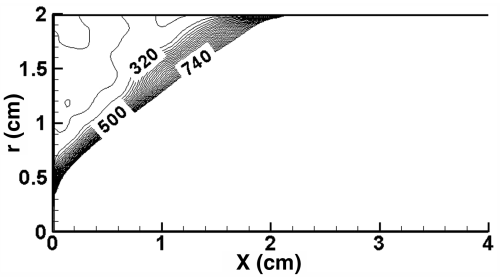

Fig. 15 Plume vibrational temperature contours using SMILE (DSMC).

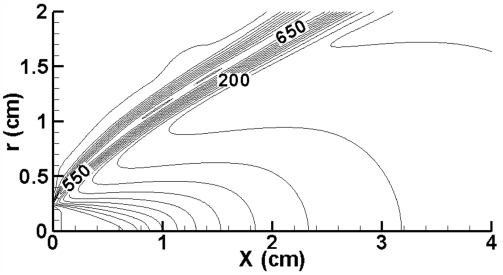

Fig. 16 Plume rotational temperature contours using UFS.

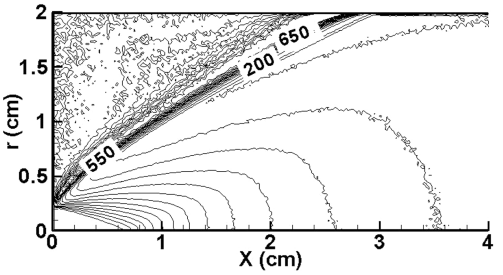

Fig. 17 Plume rotational temperature contours using SMILE (DSMC).

statistical sampling used in DSMC. The kink in the SMILE solution in the upper left corner (Fig. 13) is related to the freestream boundaries being a little too close.

The vibrational temperatures shown for UFS and SMILE in Figs. 14 and 15 are very close in magnitude, as the temperature is essentially frozen in the flowfield below the mixing layer. However, vibrational relaxation takes place across the mixing layer. Both codes predict similar vibrational temperatures in the region above the mixing layer. The SMILE results shown in Fig. 15 were smoothed to reduce the impact of the statistical scatter.

For this high-density flow, the rotational temperature fields obtained by UFS and SMILE and shown in Figs. 16 and 17 follow the same trend and magnitudes as the translational temperatures. However, the region of high rotational temperatures in the mixing

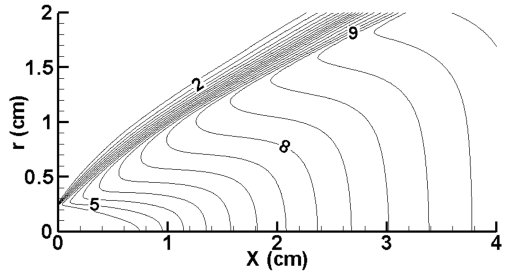

Fig. 18 Plume Mach number contours using UFS.

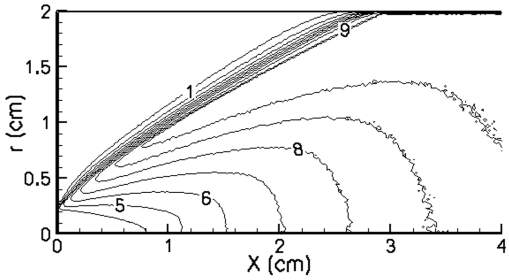

Fig. 19 Plume Mach number contours using SMILE (DSMC).

layer has a somewhat higher thickness as predicted by UFS. The Mach number contours, Figs. 18 and 19, for UFS and SMILE show a steadily increasing Mach number as the flow expands and a region above the mixing layer that approaches the background gas parameters. In the region below the mixing layer, the UFS predictions show a faster expansion with slightly higher Mach numbers. A more detailed comparison of the UFS and SMILE results are presented next.

Figures 20–24 show the axial and radial profiles of UFS and SMILE predictions of density, multitemperatures, and flow velocity in the plume region. For all the figures shown, the axial profile is along the plume centerline, and the radial profiles are at axial locations of $x = 1.15$ cm and $x = 2.37$ cm from the nozzle exit. Each of the figures is marked to show the noncontinuum region in which the UFS Boltzmann solver was used, the rest of the flowfield computed by the continuum solver.

The density profiles of UFS and SMILE along the nozzle axis are close to each other (Fig. 20a). Radial profiles of number densities predicted by both codes at $x = 1.15$ and 2.37 cm, Figs. 20b and 20c, show some difference in the magnitudes, with the maximum deviation (28%) at $x = 1.15$ cm near the centerline. The density decreases along the radial distance and beyond $x = 0.5$ cm, the density is the lowest and close to the background density. Note that the free exit boundary conditions were implemented in UFS at the top and left boundaries of the domain so that the gas is allowed to freely leave the domain.

Figure 21 shows the translational temperature profiles predicted by UFS and SMILE. Although the magnitude and trend of the centerline profiles near the nozzle exit are nearly the same, the temperature predicted by UFS is higher than that of SMILE, beyond $x = 0.6$ cm (Fig. 21a), with the maximum difference of about 10%. At $x = 1.15$ cm, the peak temperature predicted by UFS is higher by 14% than SMILE. At $x = 1.5$ cm (Fig. 21b), the UFS prediction shows a sharp equilibration with the background gas compared with the SMILE prediction, which is related to the issue of the free stream boundary for the SMILE being a little too close, discussed earlier in Fig. 13. The UFS solution also shows a slightly thicker mixing layer compared with the SMILE. At the location downstream (Fig. 21c), $x = 2.37$ cm, the peak temperature of UFS is shifted, and the mixing

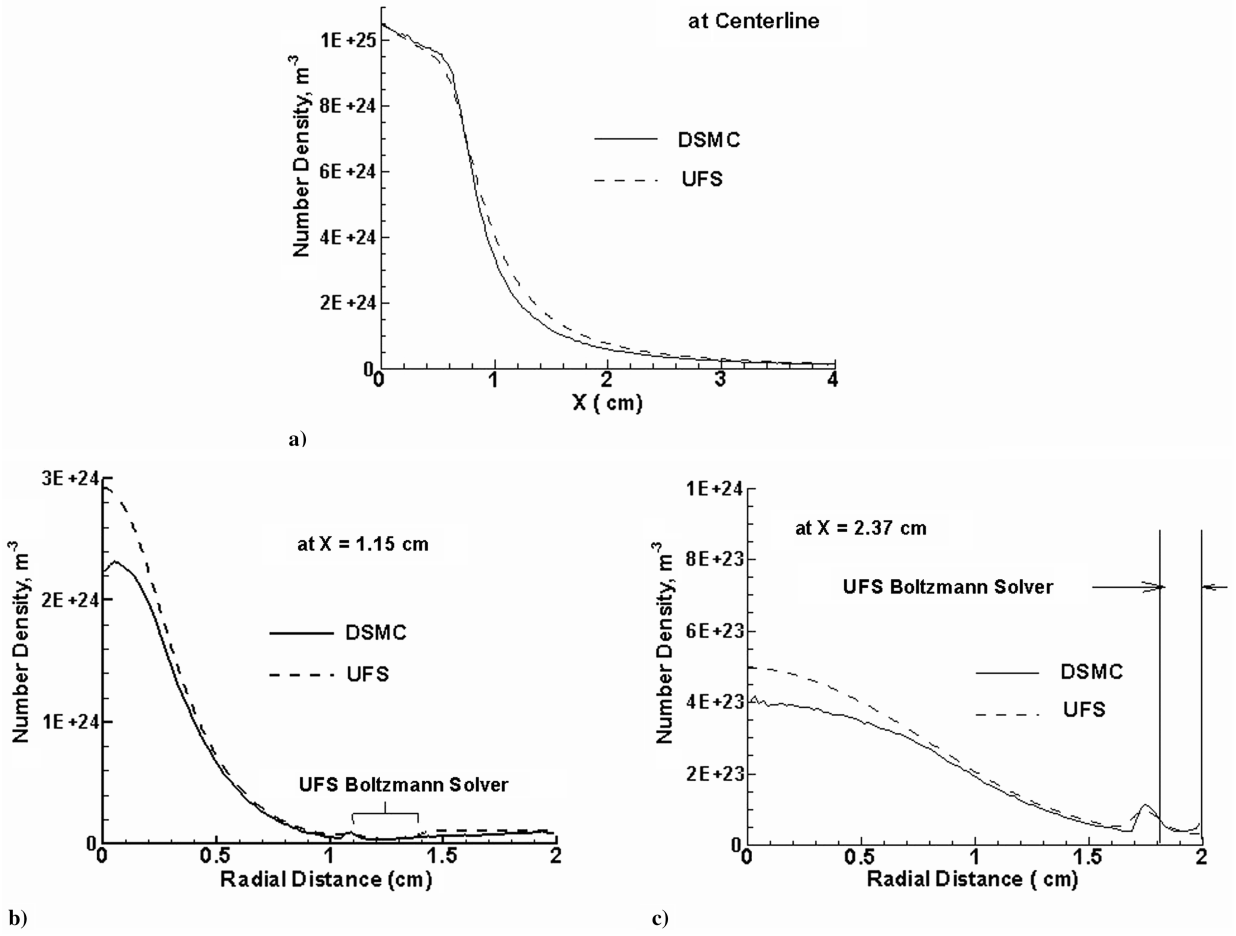

Fig. 20 Comparison of number density prediction of UFS with SMILE (DSMC) in plume region a) along centerline, b) at $x = 1.15$ cm, c) at $x = 2.37$ cm. Nozzle conditions: $T_0 = 2800$ K, $p_0 = 10,335.1$ kPa.

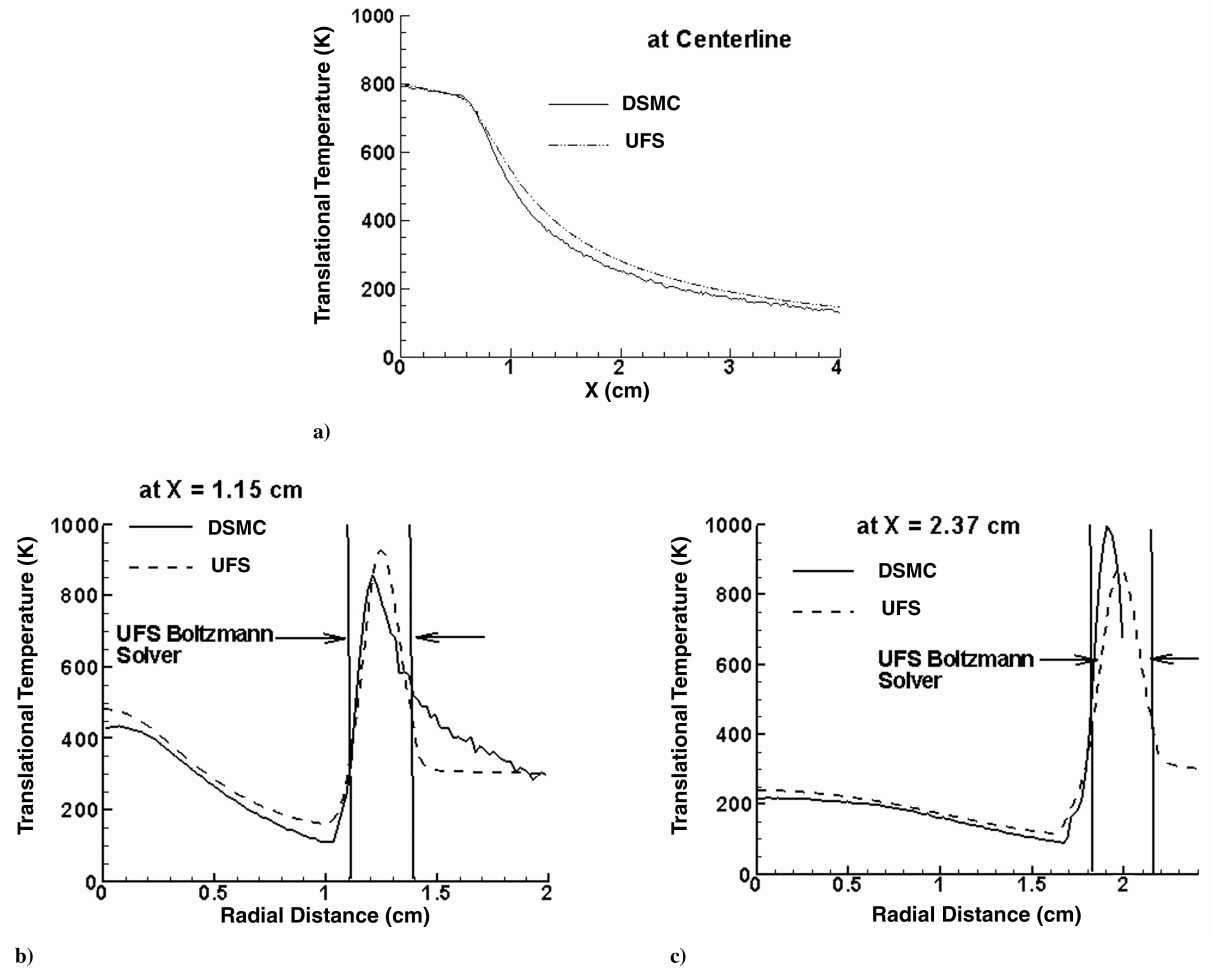

Fig. 21 Comparison of translational temperature prediction of UFS with SMILE (DSMC) in plume region a) along centerline, b) at $x = 1.15$ cm, c) at $x = 2.37$ cm. Nozzle conditions: $T_0 = 2800$ K, $p_0 = 10,335.1$ kPa.

layer predicted by UFS is thicker. In contrast to the profile at $x = 1.15$ cm, the peak temperature of SMILE at $x = 2.37$ cm is 10% higher than the UFS prediction.

The vibrational temperatures predicted by both codes, Fig. 22, are nearly the same. The vibrational temperature is frozen along the plume centerline, Fig. 22a. In the radial direction at $x = 1.15$ cm, Fig. 22b, the vibrational temperature is frozen to a distance of 1 cm from nozzle centerline and beyond this distance undergoes fast relaxation in the mixing layer with the temperature dropping rapidly. Then the relaxation slows down until the gas equilibrates at a distance of $x = 1.5$ cm. At $x = 2.37$ cm (Fig. 22c), the vibrational temperature is frozen for most of the flow (up to a radial distance of about 1.8 cm), and then undergoes rapid relaxation with a consequent drop in vibrational temperature.

Contrary to the vibrational temperature, the rotational temperature, Fig. 23, follows the translational temperature closely due to the fast relaxation between the two modes. The profiles of rotational temperatures are therefore close to those of translational temperatures. The peak rotational temperature observed at $x = 1.15$ cm (Fig. 23b), however, is the same in UFS as that in SMILE.

The axial velocity component is shown in Fig. 24. The agreement between UFS and SMILE is quite reasonable. The velocity increases along the centerline as expected due to the expansion. In the radial direction at $x = 1.15$ cm, the axial velocity component is high and undergoes a gradual decrease until a radial distance of 1 cm. Then it increases rapidly in the middle of the mixing layer and finally drops as the flow reaches the stagnant background gas. A similar behavior is seen in the radial distance at $x = 2.37$ cm, where the velocities above the mixing layer are slightly higher than those of SMILE.

Conclusions

A newly developed unified kinetic/continuum flow solver was evaluated for a high-density nozzle flow expanding into a low-density stagnant gas. The gas considered in this study is nitrogen with rotationally and vibrationally excited molecules. The UFS Boltzmann solver was used in the kinetic regions of the computational domain, and the gas-kinetic-continuum solver was used in the continuum regions. The UFS predictions of translational and vibrational temperatures in the nozzle match the existing experimental measurements within the uncertainty range.

The DSMC code SMILE was used in the plume region to provide a reference solution for UFS. From the comparisons of gas density, mean velocity, translational, rotational, and vibrational temperatures, it may be concluded that the trends of the overall flowfield were adequately captured by UFS. Comparisons between the two codes allowed the evaluation of the accuracy of UFS predictions of the location, thickness, and strength of the mixing layer; peak densities; velocity; and the multitemperatures. The UFS flowfield contours were smooth in both kinetic and continuum domains, which is not the case with SMILE contours, which showed some statistical noise.

Discrepancies were observed in the UFS and SMILE solutions at specific locations in the plume flowfield. However, the vast majority of the flowfield showed excellent agreement between the two codes. The comparison of DSMC with direct Boltzmann solver in multidimensional flow of molecular gas with internal degrees of freedom has been reported for the first time. Because the numerical methods and associated difficulties are significantly different between the DSMC and direct Boltzmann, the discrepancies observed in this study are subject to further research.

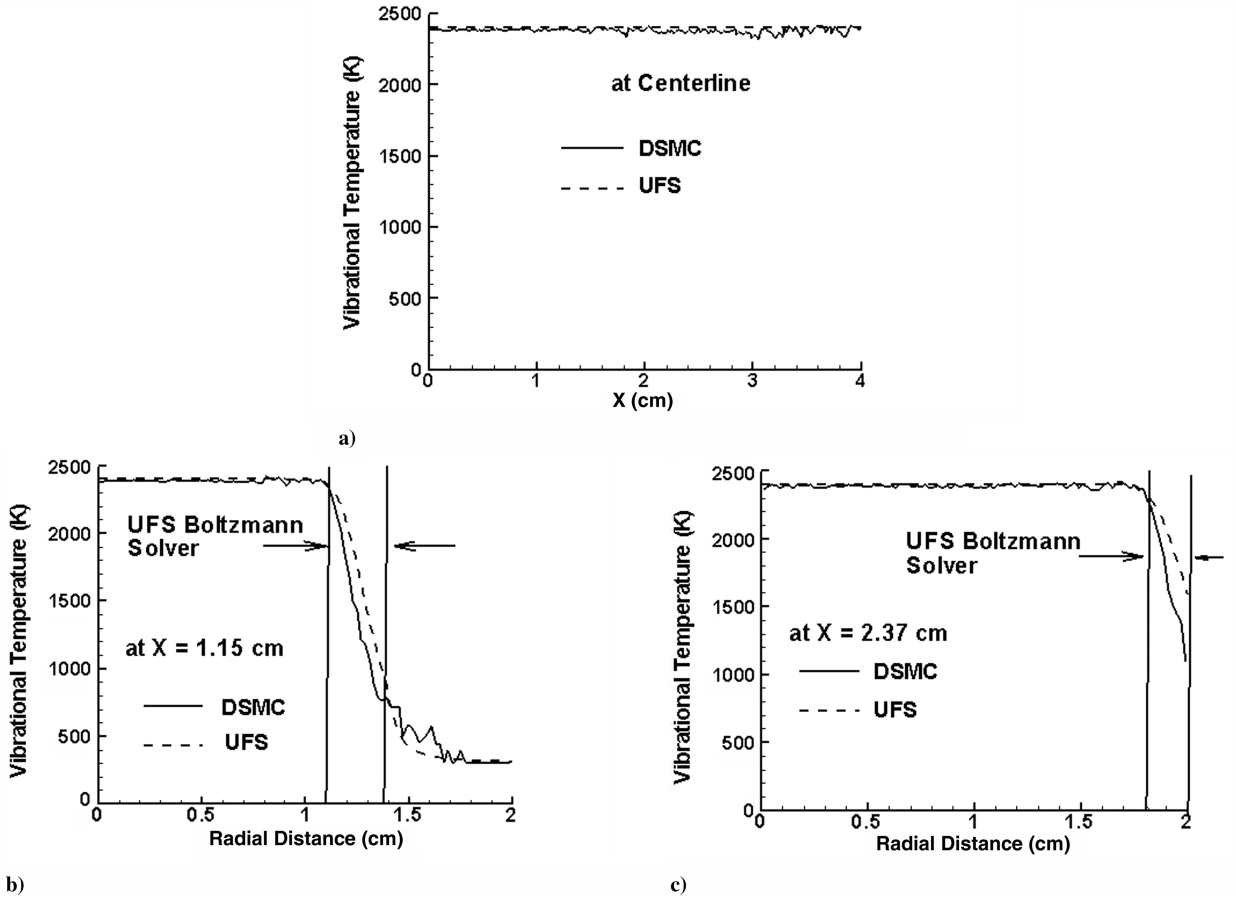

Fig. 22 Comparison of vibrational temperature prediction of UFS with SMILE (DSMC) in plume region a) along centerline, b) at $x = 1.15$ cm, c) at $x = 2.37$ cm. Nozzle conditions: $T_0 = 2800$ K, $p_0 = 10,335.1$ kPa.

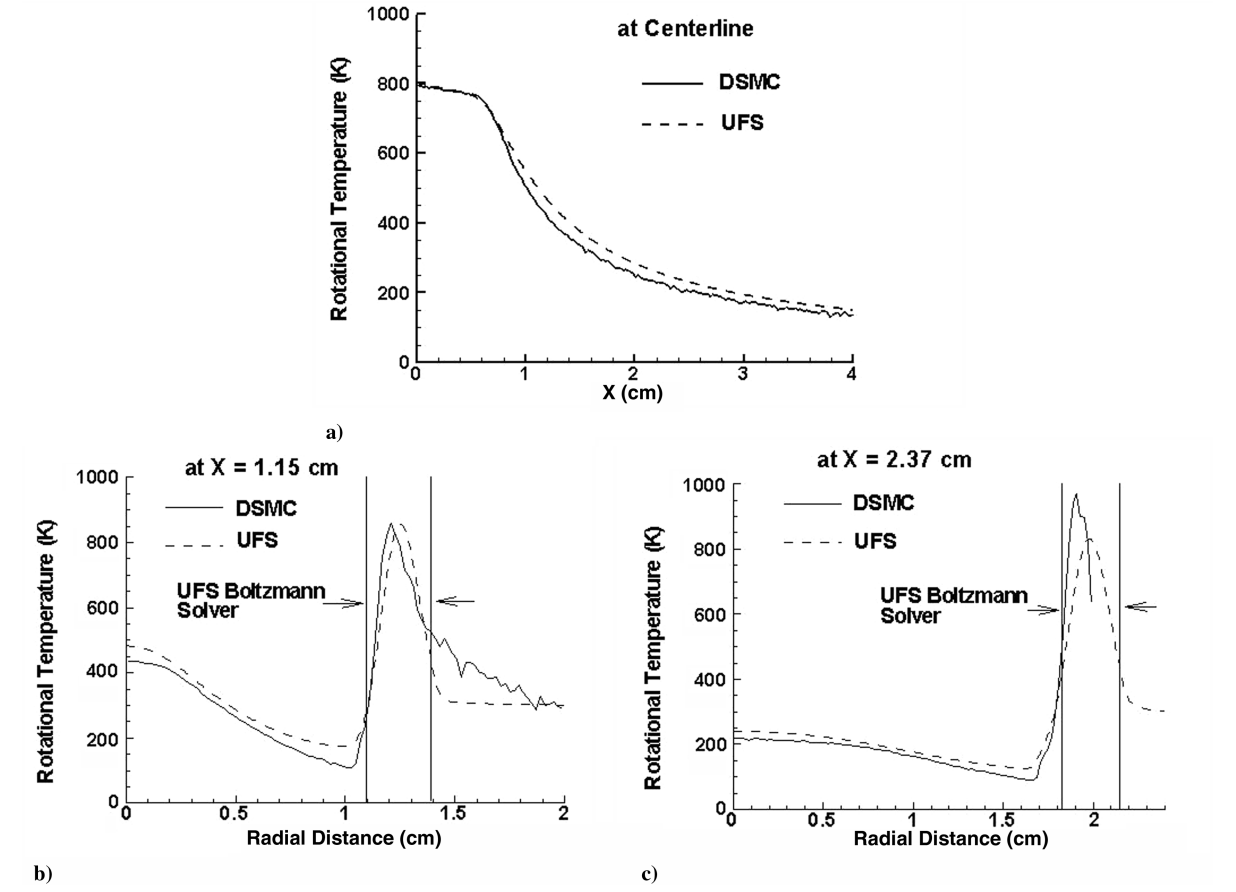

Fig. 23 Comparison of rotational temperature prediction of UFS with SMILE (DSMC) in plume region a) along centerline, b) at $x = 1.15$ cm, c) at $x = 2.37$ cm. Nozzle conditions: $T_0 = 2800$ K, $p_0 = 10,335.1$ kPa.

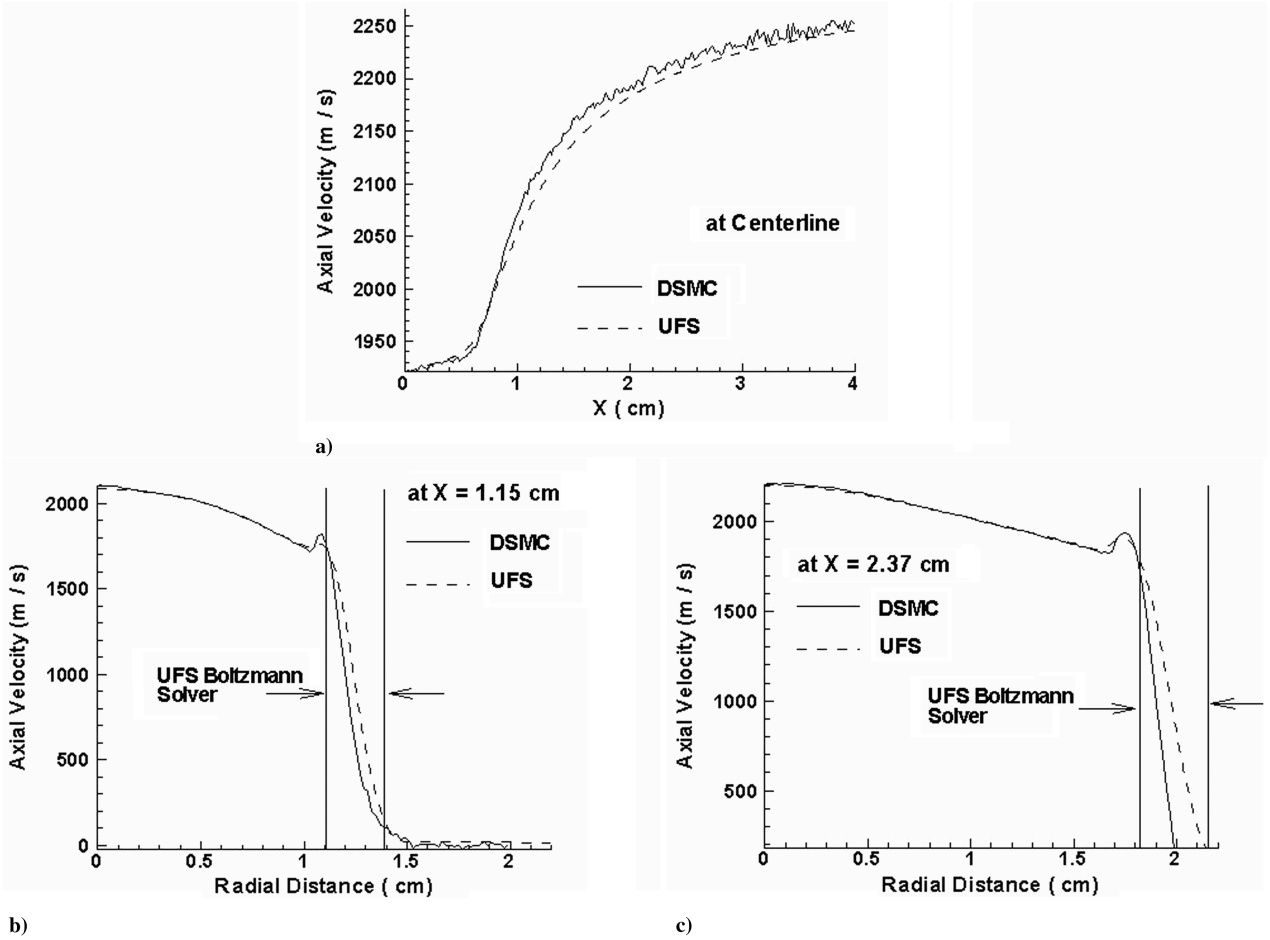

Fig. 24 Comparison of axial velocity prediction of UFS with SMILE (DSMC) in plume region a) along centerline, b) at $x = 1.15$ cm, c) at $x = 2.37$ cm. Nozzle conditions: $T_0 = 2800$ K, $p_0 = 10,335.1$ kPa.

For the highest grid resolution considered in UFS and reported in this study, the computational time is about 20% more than SMILE. The use of a continuum solver in UFS for the initial steady-state simulations could be used to accelerate the convergence of the Boltzmann solution significantly. For large continuum regions in the flowfield, the UFS solver can be faster than SMILE. However, for large kinetic domains in the flowfield, further development is needed to optimize the UFS algorithm to increase its efficiency.

Acknowledgments

Support for the first author was under U.S. Air Force Office of Scientific Research contracts monitored by F. Fahroo and J. Schmisseur. Additional support was provided by J. L. Cambier, Air Force Research Laboratory/Propulsion Directorate (AFRL/PRSA). Special thanks to A. Frolova for contributions in the UFS code development and insight. Computer resources were provided by the U.S. Department of Defense, High Performance Computing, Major Shared Resource Center, at Aeronautical Systems Center, Wright-Patterson Air Force Base, Ohio.

References

[1] Moss, J. N., Glass, C. E., Hollis, B. R., and Van Norman, J. W., "Low-Density Aerodynamics for the Inflatable Reentry Vehicle Experiment," *Journal of Spacecraft and Rockets*, Vol. 43, No. 6, Nov. 2006, pp. 1191–1201. doi:10.2514/1.22707

[2] Labbe, S. G., Perez, S., Fitzgerald, S., Longo, J. M. A., Molina, R., and Rapuc, M., "X-38 Integrated Aero- and Aerothermodynamic Activities," *Aerospace Science and Technology*, Vol. 3, No. 8, 1999, pp. 485–493. doi:10.1016/S1270-9638(99)00109-1

[3] Scwartzentruber, T. E., Scalabrin, L., and Boyd, I. D., "Hybrid Particle-Continuum Simulations of Low Knudsen Number Hypersonic Flows," AIAA Paper 2007-3892, 2007.

[4] Ivanov, M., Khotyanovski, D. V., Kudryatvtsev, A. N., Vashchenkov, P. V., Markelov, G. N., and Schmidt, A. A., "Numerical Study of Backflow for Nozzles Plumes Expanding into Vacuum," AIAA Paper 2004-2687, 2004.

[5] Boyd, I. D., Penko, P. F., Meisnner, D. L., and DeWitt, K. J., "Experimental and Numerical Investigations of Low-Density Nozzle and Plume Flows of Nitrogen," *AIAA Journal*, Vol. 30, No. 10, Oct. 1992, pp. 2453–2461.

[6] Gimelshein, S. F., Boyd, I. D., and Ivanov, M. S., "Modeling of Internal Energy Transfer in Plume Flows of Polyatomic Molecules by the DSMC Method," AIAA Paper 99-0738, 1999.

[7] Yen, S. M., "Numerical Solution of the Nonlinear Boltzmann Equation for Nonequilibrium Gas Flow Problems," *Annual Review of Fluid Mechanics*, Vol. 16, Jan. 1984, pp. 67–97. doi:10.1146/annurev.fl.16.010184.000435

[8] Muntz, E. P., "Rarefied Gas Dynamics," *Annual Review of Fluid Mechanics*, Vol. 21, Jan. 1989, pp. 387–417. doi:10.1146/annurev.fl.21.010189.002131

[9] Muntz, E. P., "Rarefied Gas Dynamics," *Research Trends in Fluid Dynamics*, edited by J. L. Lumley, J. L. Acrivos, L. G. Leal, and S. Leibovich, American Institute of Physics Press, New York, 1996, pp. 209–229.

[10] Bird, G. A., *Molecular Gas Dynamics and the Direct Simulation of Gas Flows*, Clarendon, Oxford, England, U.K., 1994.

[11] Wagner, W., "A Convergence Proof for Bird's Direct Simulation Monte Carlo Method for the Boltzmann Equation," *Journal of Statistical Physics*, Vol. 66, Nos. 3–4Feb. 1992, pp. 1011–1044. doi:10.1007/BF01055714

[12] Nanbu, K., "Direct Simulation Scheme Derived from the Boltzmann Equation. I. Multicomponent Gases," *Journal of the Physical Society of Japan*, Vol. 49, No. 5, 1980, pp. 2042–2049. doi:10.1143/JPSJ.49.2042

[13] Babovsky, H., and Illner, R., "A Convergence Proof for Nanbu's Simulation Method for the Full Boltzmann Equation," *SIAM Journal of*

Numerical Analysis, Vol. 26, No. 1, 1989, pp. 45–65.
doi:10.1137/0726004

[14] Oran, E. S., Oh, C. K., and Cybyk, B. Z., "Direct Simulation Monte Carlo: Recent Advances and Applications," *Annual Review of Fluid Mechanics*, Vol. 30, Jan. 1998, pp. 403–441.
doi:10.1146/annurev.fluid.30.1.403

[15] van Gilder, D. B., Chartrand, C. C., Papp, J., Wilmoth, R., and Sinha, N., "Computational Modeling of Nearfield to Farfield Plume Expansion," AIAA Paper 2007-5704, July 2007.

[16] Aktas, O., and Aluru, N. R., "A Combined Continuum/DSMC Technique for Multiscale Analysis of Microfluidics Filters," *Journal of Computational Physics*, Vol. 178, No. 2, 2002, pp. 342–372.
doi:10.1006/jcph.2002.7030

[17] Roveda, R., Goldstein, D. B., and Varghese, P. L., "Hybrid Euler/Particle Approach for Continuum/Rarefied Flows," *Journal of Spacecraft and Rockets*, Vol. 35, No. 3, 1998, pp. 258–265.

[18] Chen, G., and Boyd, I. D., "Statistical Error Analysis for the Direct Simulation Monte Carlo Technique," *Journal of Computational Physics*, Vol. 126, No. 2, 1996, pp. 434–448.
doi:10.1006/jcph.1996.0148

[19] Morinishi, K., "Numerical Simulation of Gas Microflows Using Boltzmann Equation," *Computers and Fluids*, Vol. 35, Nos. 8–9, 2006, pp. 978–985.
doi:10.1016/j.compfluid.2005.04.012

[20] Tcheremissine, F. G., Kolobov, V. I., and Arslanbekov, R. R., "Simulation of Shock Wave Structure in Nitrogen with Realistic Rotational Spectrum and Molecular Interaction Potential," *Rarefied Gas Dynamics: 25th International Symposium at St. Petersburg, Russia*, edited by M. S. Ivanov, and A. K. Rebrov, Siberian Branch of Russian Academy of Sciences, Novosibirsk, Russia, 2007, pp. 203–208.

[21] Kolobov, V. I., Yang, H. Q., Bayyuk, S. A., Aristov, V. V., Frolova, A. A., and Zabelok, S. A., "Unified Methods for Continuum and Rarefied Flows," AIAA Paper 2004-1177, 2004.

[22] Kolobov, V. I., Bayyuk, S. A., Arslanbekov, V. V., Aristov, R. R., Frolova, A. A., and Zabelok, S. A., "Construction of a Unified Continuum/Kinetic Solver for Aerodynamic Problems," *Journal of Spacecraft and Rockets*, Vol. 42, No. 4, July 2005, pp. 598–606.
doi:10.2514/1.10468

[23] Kolobov, V. I., Arslanbekov, R. R., Aristov, V. V., Frolov, A. A., and Zabelok, S. A., "Unified Flow Solver for Aerospace Applications," AIAA Paper 2006-988, 2006.

[24] Kolobov, V. I., Arslanbekov, R. R., Aristov, V. V., Frolova, A. A., and Zabelok, S. A., "Unified Solver for Rarefied and Continuum Flows with Adaptive Mesh and Algorithm Refinement," *Journal of Computational Physics*, Vol. 223, No. 2, May 2007, pp. 589–608.
doi:10.1016/j.jcp.2006.09.021

[25] Degond, P., Pareschi, L., and Russo, G., *Modeling and Computational Methods for Kinetic Equations*, Series on Modeling and Simulation in Science, Engineering, and Technology, Birkhäuser Boston, Cambridge, MA, 2004.

[26] Bellomo, N., and Gatignol, R., *Lecture Notes on the Discretization of the Boltzmann Equation*, Series in Advances in Mathematics for Applied Sciences, 63, World Scientific Publishing Company, River Edge, NJ, 2003.

[27] Aristov, V. V., *Direct Methods for Solving the Boltzmann Equation and Study of Non-Equilibrium Flows Phenomena*, Kluwer, Dordrecht, The Netherlands, 2001.

[28] Cercignani, C., *Boltzmann Equation and Its Applications*, Springer-Verlag, New York, 1988.

[29] Josyula, E., Xu, K., and Wadsworth, D. C., "Testing Continuum and Non-Continuum Descriptions in High Speed Flows," *Rarefied Gas Dynamics: 24th International Symposium*, CP762, American Institute of Physics, New York, 2005, pp. 1217–1222.

[30] Xu, K., and Josyula, E., "Continuum Formulation for Non-Equilibrium Shock Structure Calculation," *Computer Physics Communications*, Vol. 1, No. 3, June 2006, pp. 425–448.

[31] Kolobov, V. I., Arslanbekov, R. R., Aristov, V. V., Frolova, A. A., Zabelok, S. A., and Tcheremissine, F. G., "Unified Solver for Rarefied and Continuum Flows in Multicomponent Gas Mixtures," *Rarefied Gas Dynamics: 25th International Symposium*, edited by M. S. Ivanov and A. K. Rebrov, Siberian Branch of Russian Academy of Sciences, Novosibirsk, Russia, 2007, pp. 1035–1040.

[32] Aristov, V. V., Frolova, A. A., Zabelok, S. A., Kolobov, V. I., and Arslanbekov, R., "Application of Unified Flow Solver for Rarefied and Continuum Flows in Mixtures of Atomic and Molecular Gases," CFD Paper 33, 2007.

[33] Gillespie, W. D., "Raman Scattering Measurements of Vibrational Relaxation in Expanding Nitrogen," Ph.D. Thesis, Stanford University, Palo Alto, CA, 1993.

[34] Korobov, N. M., *Exponential Sums and Their Applications*, Kluwer, Dordrecht, The Netherlands, 1992.

[35] Popinet, S., "Gerris: A Tree-Based Adaptive Solver for the Incompressible Euler Equations in Complex Geometries," *Journal of Computational Physics*, Vol. 190, No. 2, 2003, pp. 572–600.
doi:10.1016/S0021-9991(03)00298-5

[36] Pullin, D. I., "Direct Simulation Methods for Compressible Inviscid Ideal Gas Flow," *Journal of Computational Physics*, Vol. 34, No. 2, 1980, p. 231–244.
doi:10.1016/0021-9991(80)90107-2

[37] Rykov, V. A., "Model Kinetic Equation for Gases with Rotational Degrees of Freedom," *Fluid Dynamics*, Vol. 10, No. 6, 1975, pp. 959–966.
doi:10.1007/BF01023275

[38] Titarev, V. A., Shakov, E. M., Rykov, V. A., and Soudakov, V. G., "Numerical Study of Transverse Supersonic Flow of Monatomic and Ditaomic Gases Past a Plate," *Rarefied Gas Dynamics: 25th International Symposium at St. Petersburg, Russia*, edited by M. S. Ivanov and A. K. Rebrov, Siberian Branch of Russian Academy of Sciences, Novosibirsk, Russia, 2007, pp. 274–279.

[39] Lordi, J. A., and Mates, R. E., "Rotational Relaxation in Nonpolar Diatomic Gases," *Physics of Fluids*, Vol. 13, No. 2, Feb. 1970, pp. 291–308.
doi:10.1063/1.1692920

[40] Larina, I. N., and Rykov, V. A., "Flow of a Diatomic Gas Around a Sphere on the Basis of the Kinetic Equations," *Soviet Physics–Doklady*, Vol. 21, No. 3, March 1976, pp. 117–118.

[41] Millikan, R. C., and White, D. R., "Systematics of Vibrational Relaxation," *Journal of Chemical Physics*, Vol. 39, No. 12, 1963, pp. 3209–3213.
doi:10.1063/1.1734182

[42] Ivanov, M. S., Markelov, G. N., and Gimelshein, S. F., "Statistical Q15 Simulation of Reactive Rarefied Flows: Numerical Approach and Applications," AIAA Paper 98-2669, 1998.

[43] Ivanov, M. S., and Rogasinsky, S. V., "Analysis of the Numerical Techniques of the Direct Simulation Monte Carlo Method in the Rarefied Gas Dynamics," *Soviet Journal of Numerical Analysis and Mathematical Modelling*, Vol. 3, No. 6, 1988, pp. 453–465.

[44] Borganakke, C., and Larsen, P. S., "Statistical Collision Model for Monte Carlo Simulation of Polyatomic Gas Mixture," *Journal of Computational Physics*, Vol. 18, No. 4, 1975, pp. 405–420.
doi:10.1016/0021-9991(75)90094-7

[45] Parker, J. G., "Rotational and Vibrational Relaxation in Diatomic Gases," *Physics of Fluids*, Vol. 2, No. 4, 1959, pp. 449–462.
doi:10.1063/1.1724417

[46] Lumpkin, F. E., III, Hass, B. L., and Boyd, I. D., "Resolution of Differences Between Collision Number Definitions in Particle and Continuum Simulations," *Physics of Fluids A*, Vol. 3, No. 9, 1991, pp. 2282–2284.
doi:10.1063/1.857964

[47] Park, C., "Problems of Rate Chemistry in the Flight Regimes of Aeroassisted Orbital Transfer Vehicles," *Thermal Design of Aeroassisted Orbital Transfer Vehicles*, Vol. 96, Progress in Astronautics and Aeronautics, AIAA, New York, March 1985, pp. 511–537; also AIAA Paper 1984-1730.

[48] Gimelshein, N. E., Gimeshein, S. F., and Levin, D. A., "Vibrational Relaxation Rates in the Direct Simulation Monte Carlo Method,"-*Physics of Fluids*, Vol. 14, No. 12, 2002, pp. 4452–4455.
doi:10.1063/1.1517297

[49] Gimelshein, N. E., Gimelshein, S. F., Levin, D. A., Ivanov, M. S., and Wysong, I. J., "Reconsideration of DSMC Models for Internal Energy Transfer and Chemical Reactions," *Rarefied Gas Dynamics: 23th International Symposium*, CP663, American Institute of Physics, New York, 2003, pp. 349–357.

[50] Gillespie, W. D., Bershader, D., Sharma, S. P., and Ruffin, S. M., "Raman Scattering Measurements of Vibrational and Rotational Distributions in Expanding Nitrogen," AIAA Paper 93-0274, Jan. 1993.

[51] Josyula, E., and Bailey, W. F., "Vibrational Relaxation and Population Depletion of Nitrogen in Hypersonic Flows," AIAA Paper 2002-0200, Jan. 2002.

[52] Blackman, V., "Vibrational Relaxation in Oxygen and Nitrogen," *Journal of Fluid Mechanics*, Vol. 1, No. 1, 1956, pp. 61–85.

I. Boyd
Associate Editor